THE JOURNAL OF PHYSICAL CHEMISTRY C

Article

pubs.acs.org/JPCC

# Melting of Size-Selected Aluminum Clusters with 150−342 Atoms: The Transition to Thermodynamic Scaling

Anirudh Yalamanchali, Katheryne L. Pyfer, and Martin F. Jarrold*

Chemistry Department, Indiana University, 800 E. Kirkwood Ave., Bloomington, Indiana 47405, United States

**ABSTRACT:** Heat capacities have been measured by ion calorimetry for size-selected aluminum cluster cations ranging in size from 150 to 342 atoms. All clusters show a sharp peak in their heat capacity versus temperature plots which is attributed to the melting transition. The large size dependent fluctuations in the melting temperatures found for smaller clusters in previous work have largely vanished. The melting temperatures for the 150−342 atom size range examined here are substantially below the bulk value and increase relatively smoothly with size. Above 180 atoms, they closely follow the $1/r$ dependence predicted by thermodynamic models. A notable exception occurs between $Al_{283}^+$ and $Al_{284}^+$, where the melting temperature suddenly jumps by 13 K. This jump represents a remarkably sudden change for such large clusters. The origin is probably structural, but the nature of the structural change remains unknown. The latent heat is still far from its bulk value (only 42%) even for the largest clusters studied here. When the data for aluminum clusters and particles are combined, melting temperatures are available over a size range spanning 6 decades, providing a complete picture of how the melting temperature changes with size.

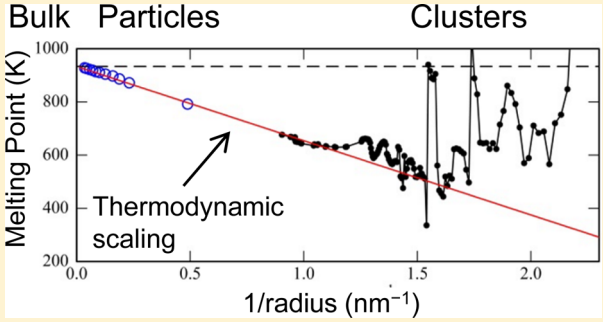


## INTRODUCTION

With their size-dependent reactivity, optical properties, and thermodynamic properties, nanoparticles have been studied extensively for potential applications, including those to energy, catalysis, and medicine.[1,2] As predicted by Pawlow in 1909, particles composed of 1000s of atoms have depressed melting points due to their increased surface-area-to-volume ratio.[3−10] Such a relationship has been difficult to establish for clusters (<1000 atoms). Adding an atom to a small cluster can cause a dramatic change in the melting temperature,[11,12] and the size range where the melting temperatures of the clusters start to follow the thermodynamic scaling of the particles is not known.

Most of the information on the melting of metal clusters has been obtained from calorimetry measurements on isolated, size-selected clusters in the gas phase. Several methods have been developed to perform these measurements.[13−15] Basically, heat capacities are recorded as a function of temperature, and a peak in the heat capacity signals the melting transition. The location of the peak provides the melting temperature, and the area is the latent heat. A few metal clusters show more complicated behavior, such as curves with more than one peak or with a dip and a peak.[16−20] A dip in the heat capacity is due to a transition to a lower enthalpy solid prior to melting.[18] When there is a second peak, it could be due to either partial melting of the cluster or a transition to a higher enthalpy solid.[16,17] Annealing studies can help to distinguish between these possibilities.[20]

The melting of sodium,[11,13,21−24] gallium,[14,25,25−29] and aluminum[16−18,20,30−35] clusters has been extensively studied. There have also been studies of tin clusters,[36,37] sodium chloride clusters,[38] and deprotonated water clusters.[39] Sodium clusters have melting temperatures that are well below the bulk value. There has been a lot of interest in the size-dependent variations in the melting temperatures of sodium clusters. Local maxima have been attributed to geometric and electronic shell closings.[40,41] Several related phenomena have been observed with sodium clusters, including melting point depression by insoluble impurities[42] and a negative heat capacity.[43] In contrast to sodium, small gallium clusters have melting temperatures substantially above the bulk value.[14,29,44] Some gallium clusters melt without a well-defined peak in the heat capacities,[26] while others show sharp peaks. Molecular dynamic simulations suggest that the sharp peaks result from relatively ordered ground state geometries.[45] Studies with density functional theory (DFT) suggest that the structural motif of the global minimum-energy structure affects the melting temperatures. Thus, the more spherical ground states of gallium clusters with between 43 and 48 atoms is responsible for their significantly higher melting temperatures than smaller clusters with 31−39 atoms.[46]

The melting of small aluminum clusters is characterized by large size-dependent fluctuations in the melting temperatures. Except for a few small clusters, the melting temperatures are below the bulk melting point. Aluminum clusters have been the subject of several studies where the reactivity of liquid and solid clusters was compared. For example, the chemisorption of $N_2$ has been studied both experimentally and through DFT and molecular dynamics simulations.[47−49] The kinetic energy thresholds for chemisorption of $N_2$ were lower for the liquid

**Received:** March 23, 2017
**Revised:** April 20, 2017
**Published:** May 2, 2017





DOI: 10.1021/acs.jpcc.7b02768
J. Phys. Chem. C 2017, 121, 10242−10248

cluster than the solid cluster for $Al_{44}^{\pm}$ and $Al_{100}^{+}$, but not for $Al_{114}^{+}$, $Al_{115}^{+}$, and $Al_{117}^{+}$. Further differences in the chemistry of liquid aluminum clusters versus their solid counterparts were observed in the reactivity of $CO_2$ and benzene with $Al_{100}^{+}$.[50,51]

A number of computational studies have been performed to understand the melting of aluminum clusters ranging in size from tens of atoms to a few hundred atoms.[52−59] In addition, some studies have examined larger clusters, with hundreds or even thousands of atoms.[60−62] According to the simulations of Alavi and Thompson,[60] particles with less than 850 atoms show bistability near the melting transition, where the clusters fluctuate between solid and liquid, while clusters with more than 850 atoms undergo a sharp solid−liquid phase transition reminiscent of the bulk phase transition. Ojwang et al. used the parametrized reactive force field model and concluded that aluminum clusters with $n \leq 55$ favor icosahedral order, clusters with $256 \leq n \leq 1024$ favor mixed hcp−fcc order, and clusters with $n \geq 1024$ prefer fcc order. However, DFT calculations suggest icosahedral isomers have very high energies for small clusters (including $Al_{55}$) and find that bulk-like fcc order emerges at much smaller cluster sizes.[34,63] In this paper we present melting temperatures and latent heats measured for size-selected aluminum clusters with between 150 and 342 atoms. This work extends our previous measurements on the melting of aluminum clusters with between 16 and 128 atoms[16,17,30,35] and fills in some of the gap between the cluster measurements and measurements with aluminum particles.[4]

## EXPERIMENTAL METHODS

A diagram of the main components of the experimental apparatus is shown in the upper half of Figure 1.[30] The lower half of Figure 1 shows the main steps involved in determining the melting temperatures for size-selected cluster ions. Aluminum cluster ions were generated by pulsed laser (248 nm, 100 Hz) vaporization of a liquid aluminum target in a continuous flow (400 sccm) of ultrahigh-purity helium. A liquid target is used in place of a solid because holes generated by laser ablation are constantly filled in, maintaining signal stability.[64] The source region is cooled to 273 K to encourage cluster growth.

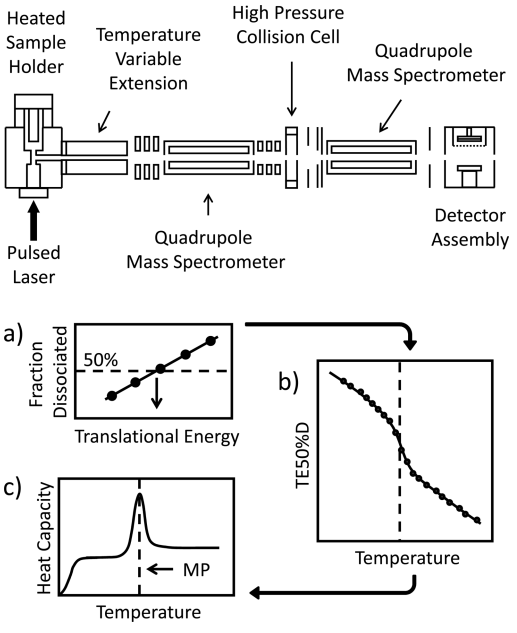


**Figure 1.** Upper half shows a diagram of the main components of the experimental apparatus. The lower half shows the main steps involved in measuring melting temperatures for size-selected cluster ions.

The helium buffer carries the aluminum clusters into a 10 cm long, temperature-variable extension where the temperature of the clusters is set. The temperature of the extension is regulated by a programmable microcontroller. The clusters undergo enough collisions to equilibrate to the temperature of the extension. After exiting the extension through a small aperture, the cluster cations are focused and accelerated into the first quadrupole mass filter (QMF).

The QMF selects a specific cluster size. The size-selected clusters are then accelerated and focused into the collision cell which contains 0.400 Torr of neon gas. The cluster ions undergo a series of collisions with the neon gas until eventually the cluster's translational energy is thermalized. In each collision, a small fraction of the cluster's translational energy is converted into internal energy. Once the clusters translational energy is thermalized, further collisions reduce the internal energy of the cluster until eventually the internal energy is also thermalized. Thus, the clusters undergo a transient heating and cooling cycle after injection into the collision cell. If their internal energy becomes high enough during this cycle, they may dissociate. The only dissociation process observed is evaporation of individual aluminum atoms. At high initial translational energies multiple evaporation steps are observed.

A weak electric field guides the undissociated cluster ions and fragment ions across the collision cell. Some of them exit via a small aperture and are focused into a second QMF. The second QMF is used to measure the $m/z$ spectrum. Ions transmitted by the QMF are detected by a collision dynode and dual microchannel plate assembly.

The $m/z$ spectra are analyzed to determine the fraction of clusters that dissociate. Measurements are performed as a function of the initial translational energy, and a linear regression is used to determine the translational energy at which 50% of the clusters dissociate (TE50%D) (as illustrated in Figure 1a). TE50%D is then determined for a variety of initial cluster temperatures to determine how the internal energy of the cluster changes with temperature. As the initial temperature is raised (by increasing the temperature of the extension), the clusters' internal energy increases, and less energy must be added to the clusters to achieve 50% dissociation. At the melting temperature, where the latent heat causes the internal energy to increase suddenly, there is a sudden drop in the TE50% value (as illustrated in Figure 1b). The cluster's heat capacity is given by

$$C(T) = F \times -\frac{\Delta \mathrm{TE50\%D}}{\Delta T} \quad (1)$$

where the proportionality constant, $F$, is the fraction of the cluster's translational energy that is converted into internal energy during a collision. $F$ is calculated using an impulsive collision model.[65,66] A plot of the heat capacity against temperature shows a peak that is attributed to the melting transition (as illustrated in Figure 1c).

## RESULTS

Heat capacities were determined as a function of temperature for 35 $Al_n^{+}$ clusters with $150 \leq n \leq 342$ atoms. Representative plots of heat capacity versus temperature are shown in Figure 2 for clusters with $n = 150$ and 192. The measured heat capacities



DOI: 10.1021/acs.jpcc.7b02768
J. Phys. Chem. C 2017, 121, 10242−10248

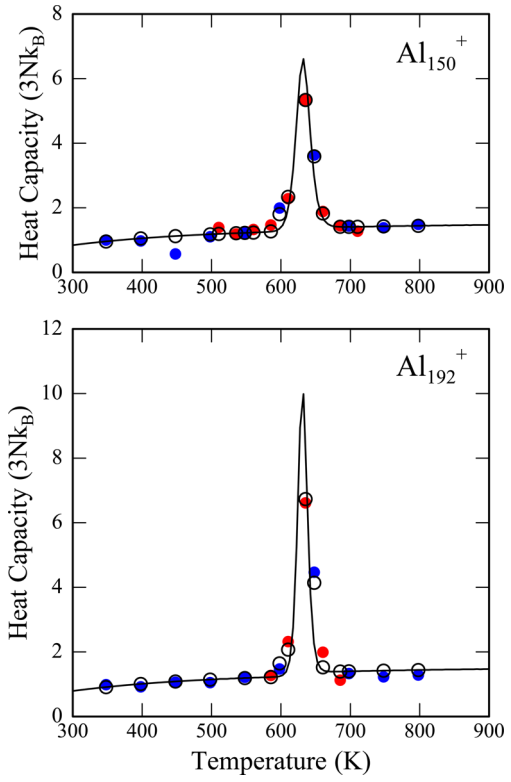


**Figure 2.** Heat capacities measured as a function of temperature for $Al_{150}^+$ and $Al_{192}^+$. The heat capacities are plotted in units of $3Nk_B$ where $N = (3n - 6 + 3/2)$, $k_B$ is the Boltzmann constant, $(3n - 6)$ is the vibrational component, and $(3/2)$ is the rotational component. The filled blue and red points are the measured values with $\Delta T = 50$ K and $\Delta T = 25$ K, respectively. The unfilled black circles are fits to the measured values using the two-state model (see text). The black lines are the heat capacities calculated with the two-state model using $\Delta T = 5$ K and the melting temperature and latent heat from the fit to the measured values.

are plotted in units of $3Nk_B$, where $N = (3n - 6 + 3/2)$, $k_B$ is the Boltzmann constant, and $3n - 6$ and $3/2$ are the vibrational and rotational contributions, respectively. The filled blue and red points in Figure 2 are the measured values (the average of at least three independent measurements) determined with $\Delta T = 50$ K and with $\Delta T = 25$ K, respectively. Initial measurements, to locate the melting transition, were performed with $\Delta T = 50$ K, and then further measurements were made with $\Delta T = 25$ K to better resolve the peak in the heat capacity. Ideally, it would be better to use even smaller values of $\Delta T$. However, when $\Delta T$ is reduced, the uncertainty in the heat capacity measurement increases (because of increased uncertainties in $\Delta T$ and $\Delta$TE50%D), and we judged that it was better to use larger values of $\Delta T$ and then fit the data to determine the melting temperature.

The plots of heat capacity versus temperature were fit with the two-state model described previously.[17,67] In this model, it is assumed that phase coexistence at the melting transition is dynamic; in other words, clusters at the melting temperature rapidly switch between being fully solid and fully liquid, rather than the two phases coexisting in contact as they do in the bulk. According to the molecular dynamics simulations of Alavi and Thomson,[60] the melting of aluminum nanoparticles remains two state (dynamic coexistence melting) up to around 850 atoms whereupon the melting transition switches to bulk-like behavior. In the two-state model used to fit the measured heat capacities, the underlying heat capacity of the solid cluster is obtained from a modified Debye model which includes a low-frequency cutoff to account for the finite size of the clusters.[59] The heat capacity of the liquid cluster is assumed to be larger than the solid due to the extra configurational entropy. The predictions of the model are fit to the experimental results using a least-squares criterion to optimize the melting temperature, the latent heat, and the difference between the heat capacities of the liquid and solid. In our previous work, some aluminum clusters had two peaks or a bimodal peak in the heat capacity plots. Multiple peaks indicate the presence of an intermediate, and in those cases the results were fit using a three-state model.[17,20] However, only a single peak was found for the clusters studied here, and the two-state model was satisfactory for all of them.

The unfilled black circles in Figure 2 are calculated fits to the experimental data points using the two-state model described above. The solid black line was generated using the melting temperature and latent heat from the fits, but with a temperature increment of $\Delta T = 5$ K. From the fits in Figure 2, the melting temperatures for $Al_{150}^+$ and $Al_{192}^+$ are almost the same (632 and 631 K, respectively). The latent heats (512 kJ/mol for $Al_{150}^+$ and 758 kJ/mol for $Al_{192}^+$) show a systematic increase with cluster size. This increase leads to a systematic narrowing of the peak in the heat capacity that is evident from the data in Figure 2 for just $Al_{150}^+$ and $Al_{192}^+$.

There is generally good agreement between measured heat capacities and heat capacities from the best fit of the two-state model. A notable exception in Figure 2 is the point for $Al_{150}^+$ at around 450 K where the measured point is significantly below the predictions of the model and below the values of neighboring points. For some of the smaller aluminum clusters studied in our previous work, we observed dips in the heat capacity versus temperature plots (below the melting transition) which were attributed to structural transitions to higher energy (but higher entropy) structures.[18] It is likely that this is the explanation for the apparent discrepancy at 450 K for $Al_{150}^+$.

Melting temperatures determined from the fits of the two-state model are shown in Figure 3. The upper half of Figure 3 shows the melting temperatures (blue points) determined in this work. The lower half of Figure 3 shows a compilation of melting temperatures determined for size-selected aluminum clusters from this work and our earlier studies for $n = 24$–128.[16,17,30,31,35] The black lines connecting the points are guides. The large size-dependent fluctuations in the melting temperatures observed for aluminum clusters with less than 100 atoms have vanished in the size range examined in this work. The only notable feature for clusters with 150–342 atoms is the ~13 K jump in the melting temperature that occurs between clusters with 283 and 284 atoms. The absolute uncertainty in the melting temperatures reported here is ±5 K. However, the relative uncertainties are considerably lower, and we are confident that the ~13 K jump between $Al_{283}^+$ and $Al_{284}^+$ is a real feature and its location is correctly identified.

The area under a peak in the heat capacity versus temperature plots (or equivalently, the step in the TE50%D values versus temperature) is the latent heat. The upper half of Figure 4 shows the latent heat per atom plotted against cluster size. Results are shown for all clusters with $24 \leq n \leq 342$. For the new measurements, $150 \leq n \leq 342$, the latent heats increase slowly with cluster size with little size-dependent variation. The inset shows an expanded view of the region


DOI: 10.1021/acs.jpcc.7b02768
J. Phys. Chem. C 2017, 121, 10242–10248

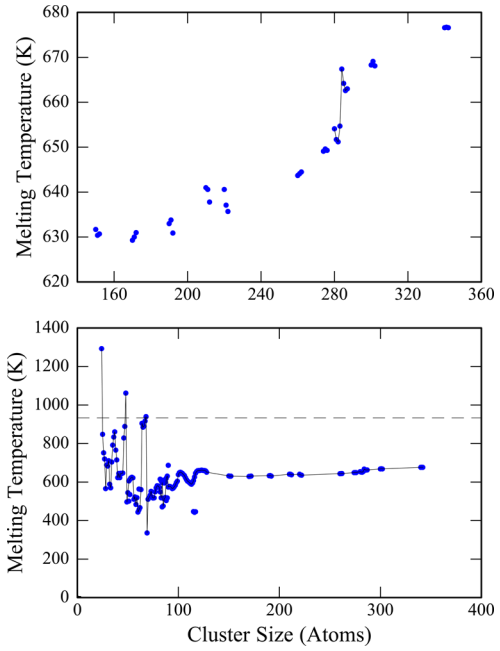


**Figure 3.** Upper panel shows melting temperatures obtained from the two-state fit as a function of size for clusters with 150−342 atoms. The absolute uncertainty in the melting temperatures is ±5 K, and the relative uncertainty is considerably lower. The lower panel shows a plot of the melting temperatures reported here for clusters with 150−342 atoms combined with those measured in previous work for clusters with 24−128 atoms.[16,17,30,31,35] The thin solid lines are guides. The dashed horizontal value shows the bulk melting point.

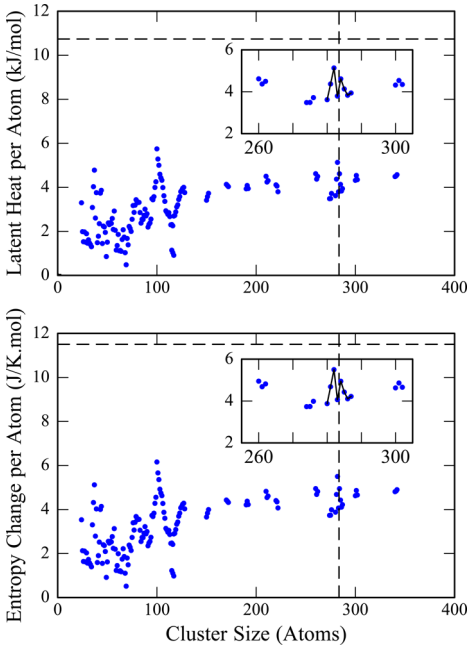


**Figure 4.** Upper panel shows the latent heat per atom plotted against cluster size for the measurements reported here (150−342 atoms) and from previous measurements for smaller sizes (24−128 atoms). The dashed horizontal line shows the bulk value, and the inset shows an expanded view around the jump in melting temperature that occurs between 283 and 284 atoms. The dashed vertical line indicates the location of the jump. The lower panel shows a similar plot of the entropy change per atom.

around 283−284 atoms where the melting temperature jumps. There are maxima at both $Al_{282}^+$ and $Al_{284}^+$, but changes in the latent heats do not appear to be correlated with the jump in melting temperature. The latent heats for clusters near to the jump appear to be significantly lower relative to clusters further away. The dashed horizontal line in upper half of Figure 4 shows the bulk value for the latent heat (10.74 kJ/mol). Even for the largest clusters studied here the latent heats are only around 42% of the bulk value.

The entropy changes for the melting transitions were calculated from

$$\Delta S_m = \frac{\Delta H_m}{T_m} \quad (2)$$

where $\Delta H_m$ is the latent heat and $T_m$ is the melting temperature. The entropy changes per atom are shown in the lower half of Figure 4. The entropy changes track the latent heats quite closely. Enthalpy−entropy compensation has been observed for sodium cluster melting as well.[22,68] Because of this compensation, the relative fluctuations in the melting temperatures are less than the relative fluctuations in the latent heats. The variations in the entropy change around the melting temperature jump between $n$ = 283 and 284 also track the variations in the latent heats, with maxima at both $Al_{282}^+$ and $Al_{284}^+$. The horizontal dashed line in the lower half of Figure 4 shows the bulk value for the entropy of melting (11.50 J $K^{-1}$ $mol^{-1}$). For the largest clusters studied here the entropy of melting is around 58% of the bulk value.

## DISCUSSION

In general, the peaks in the heat capacity plots became sharper (both narrower and taller) with increasing cluster size (see Figure 2). This behavior is a direct consequence of the latent heat of the cluster increasing with increasing cluster size and reflects the transition to bulk-like behavior where melting ultimately occurs at a single well-defined melting point. The narrowing of the peaks with increasing cluster size indicates that the solid-like and liquid-like states coexist over a narrower temperature range.

The melting temperatures in the lower half of Figure 3 can be divided into three domains. Small clusters, with less than 90 atoms, have erratic melting temperatures which fluctuate over a 700 K range. Medium sized clusters, with between 90 and 128 atoms, show a smooth, oscillatory pattern spanning about 100 K. The large clusters above 150 atoms measured in this study show a pattern of smoothly increasing melting temperature. The dashed horizontal line in the lower half of Figure 3 shows the bulk melting point. The melting temperatures of the largest clusters studied here are still only 72% of the bulk value. For these clusters, the latent heats are 42% of the bulk value and the entropy of melting is 58%. For clusters with depressed melting temperatures, the entropy changes must necessarily approach the bulk value more rapidly than the latent heats.

With the new results presented here, melting temperatures are now available for aluminum clusters over a broad range of sizes. Melting temperatures have also been determined for supported aluminum particles, and it is instructive to compare the two data sets. This comparison is shown in the upper half of Figure 5, where the melting temperatures are plotted against 1/$r$. The radius, $r$, is given by


DOI: 10.1021/acs.jpcc.7b02768
J. Phys. Chem. C 2017, 121, 10242−10248

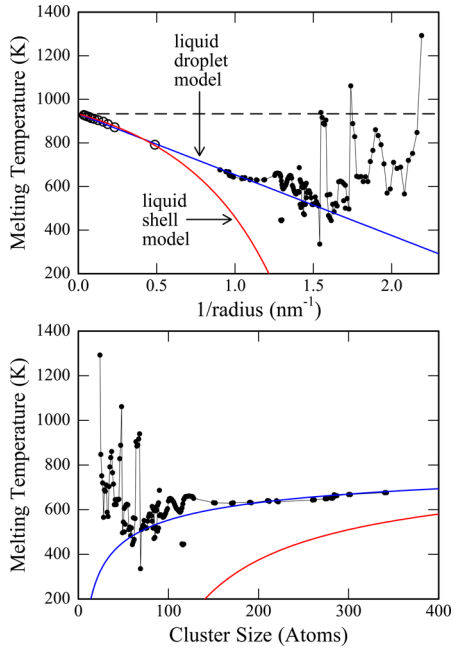


**Figure 5.** Upper panel shows melting temperatures measured for size selected aluminum clusters (filled points) and melting temperatures measured for supported particles (open circles) from ref 9. The lines show the predictions of thermodynamic models. The red line is the prediction of the liquid shell model, and the blue line is the prediction of the liquid droplet model (see text for a description of both models). The lower panel shows an expanded view of the comparison with the thermodynamic models in the cluster size regime.

$$r = \left(\frac{3nV_a}{4\pi}\right)^{1/3} \tag{3}$$

where $V_a$ is the volume of an atom in the bulk metal. The filled points in the upper half of Figure 5 are the cluster measurements, and the open circles are melting temperatures measured for supported aluminum particles by Lai et al.[4] While there is not direct overlap between the two sets of measurements, the gap between them is relatively small. This is the first time that it has been possible to examine the melting temperatures over such a broad size range (6 decades). For the larger particles ($n > 10^6$) the melting temperatures have almost attained the bulk value (dashed horizontal line).

A variety of models have been proposed using thermodynamic arguments to rationalize the size-dependent melting behavior of small particles. These models point to the surface as the cause of depressed melting points for small particles. In the liquid shell model, melting is assumed to start with a thin liquid shell in equilibrium with a solid core. When the shell thickness reaches a critical value, the whole particle melts. The melting temperature depression predicted by this model is[4,6,7]

$$T_m^\infty - T_m = \frac{2T_m^\infty}{\Delta H_m^\infty}\left[\frac{\gamma_{SL}}{\rho_S(r-t)} + \left(\frac{\gamma_L}{r} + \frac{\Delta P}{2}\right)\left(\frac{1}{\rho_S} - \frac{1}{\rho_L}\right)\right] \tag{4}$$

where $T_m^\infty$ is the melting point of the bulk, $t$ is the critical thickness of the liquid layer, $\rho_{SL}$ is the interfacial energy between the bulk solid and liquid at $T_m^\infty$, and $\Delta P = P^\infty - P$, where $P$ is the vapor pressure at the spherical surface of the liquid particle at its melting temperature (determined from the Kelvin equation) and $P^\infty$ is the vapor pressure at the planar surface of the bulk liquid at $T_m^\infty$. For aluminum, the term containing $\Delta P$ is much smaller than the term containing $\rho_L$ (because of the low vapor pressure of aluminum), except for exceedingly small clusters (<15 atoms).

In the liquid droplet model it is assumed that solid particles and liquid particles are in equilibrium with the vapor and that melting involves a transition between the solid and liquid particles (i.e., there is no surface premelting). With this model the melting temperature depression is given by[3,5,8]

$$T_m^\infty - T_m = \frac{2T_m^\infty}{\Delta H_m^\infty \rho_S r}\left[\gamma_S - \gamma_L\left(\frac{\rho_S}{\rho_L}\right)^{2/3}\right] \tag{5}$$

where $T_m^\infty$ is the melting point of the bulk, $\Delta T_m^\infty$ is the latent heat for the bulk, $r$ is the particle radius, $\gamma_S$ and $\gamma_L$ are the surface energies of the bulk solid and liquid at the bulk melting point, and $\rho_S$ and $\rho_L$ are the densities of the bulk solid and liquid at the bulk melting point.

In order to compare to the predictions of the preceding models, values are required for $\rho_L$, $\rho_S$, $\gamma_L$, $\gamma_S$, and $\gamma_{SL}$. Reliable values are available for $\rho_L$ (2377 kg/m$^3$),[69] $\rho_S$ (2551 kg/m$^3$),[70] and $\gamma_L$ (0.943 J/m$^2$).[71] When reliable values were not available, the parameters were determined by manually fitting the predictions of the models to the experimental results. The liquid shell model is most appropriate for larger particles, so the predictions of this model were fit to the results of Lai et al.[4] (open circles in Figure 5) by adjusting $\gamma_{SL}$ and $t$. $\gamma_{SL}$was determined mainly by the fit to the larger particles and $t$ by the fit to the smaller ones. The predictions of the liquid shell model are shown by the red lines in Figure 5. The values of $\gamma_{SL}$ and $t$ employed were 0.18 J/m$^2$ and 0.45 nm.

The liquid droplet model is most appropriate for large clusters (or very small particles) that are expected to show dynamic phase coexistence. Thus, the predictions of this model were fit to the measurements for the larger clusters by adjusting the value of $\gamma_S$. The predictions of the liquid droplet model are shown by the blue lines in Figure 5. The value of $\gamma_S$ employed was 1.4 J/m$^2$. The liquid droplet model provides a good fit to the melting temperatures measured for aluminum clusters with more than around 180 atoms. The liquid droplet model also provides a good fit to the melting temperatures of the particles, though it underestimates the melting temperatures for the larger particles by slightly more than the liquid shell model. The values of $\gamma_{SL}$ and $\gamma_S$ deduced here are in line with expectations that $\gamma_S > \gamma_L + \gamma_{SL}$, which is a consequence of the fact that metals (including aluminum) cannot be superheated.[72]

The only notable variation in the smooth increase in the melting temperatures for clusters with more than 150 atoms is the 13 K jump in the melting temperature that occurs between $Al_{283}^+$ and $Al_{284}^+$. The jump represents a remarkably sudden change in a physical property for such large clusters. While the jump does not have an overt signature in the latent heats or entropies of melting, the latent heats and entropies for clusters near the jump are depressed relative to values for clusters further from the jump. For smaller clusters, such sudden jumps in melting temperature have been attributed to either electronic or geometric shell closings.[61] However, we are not aware of a model that predicts a shell closing for aluminum clusters with between 283 and 284 atoms. The cause of the jump is most likely a structural change. This is consistent with the local depression of the latent heats and entropies before the jump. However, our results provide no insight into the nature of the structural change.



DOI: 10.1021/acs.jpcc.7b02768
J. Phys. Chem. C 2017, 121, 10242−10248

## CONCLUSION

Ion calorimetry measurements have been performed for aluminum cluster cations with between 150 and 342 atoms. In contrast to the wild fluctuations in melting temperature for small aluminum clusters, the clusters in this study showed a relatively smooth increase in melting temperature with increasing cluster size. The main exception to this global behavior is a sudden 13 K jump in the melting temperature between $Al_{283}^+$ and $Al_{284}^+$. The jump probably results from a structural change. For clusters with more than 180 atoms the melting temperatures follow the $1/r$ dependence predicted by thermodynamic models which can account for the melting temperature depression of much larger particles. Thus, the size range examined here is the regime where thermodynamic scaling emerges. The breakdown in thermodynamic scaling that occurs for clusters with less than 180 atoms reflects a transition to the size regime where properties start to depend strongly on the precise number of atoms in the cluster. Such a transition is expected; the results presented here provide a fine illustration of this behavior. When the data for aluminum clusters and particles are combined, melting temperatures are available over a size range spanning 6 decades, providing a complete picture of how the melting temperature changes with size.

## AUTHOR INFORMATION


### Corresponding Author

*E-mail mfj@indiana.edu (M.F.J.).

### ORCID

Martin F. Jarrold: 0000-0001-7084-176X


### Notes

The authors declare no competing financial interest.

## ACKNOWLEDGMENTS

We gratefully acknowledge the support of the US National Science Foundation under Grant CHE-0911462.

## REFERENCES


(1) Schmid, G.; Bäumle, M.; Geerkens, M.; Heim, I.; Osemann, C.; Sawitowski, T. Current and Future Applications of Nanoclusters. *Chem. Soc. Rev.* **1999**, *28*, 179−185.

(2) Ferrando, R.; Jellinek, J.; Johnston, R. L. Nanoalloys: From Theory to Application of Alloy Clusters and Nanoparticles. *Chem. Rev.* **2008**, *108*, 845−910.

(3) Pawlow, P. Über die Abhängigkeit des Schmelzpunktes von der Oberflächenenergie eines Festen Körpers. *Z. Phys. Chem.* **1909**, *65*, 1−35.

(4) Reiss, H.; Wilson, I. B. The Effect of Surface on Melting Point. *J. Colloid Sci.* **1948**, *3*, 551−561.

(5) Hanszen, K. J. Theoretische Untersuchungen über den Schmelzpunkt Kleiner Kügelchen: Ein Beitrag zur Thermodynamik der Grenzfliiehen. *Eur. Phys. J. A* **1960**, *157*, 523−553.

(6) Wronski, C. R. M. The Size Dependence of the Melting Point of Small Particles of Tin. *Br. J. Appl. Phys.* **1967**, *18*, 1731−1737.

(7) Coombes, C. J. The Melting of Small Particles of Lead and Indium. *J. Phys. F: Met. Phys.* **1972**, *2*, 441−449.

(8) Buffat, Ph.; Borel, J.-P. Size Effect on the Melting of Gold Particles. *Phys. Rev. A: At., Mol., Opt. Phys.* **1976**, *13*, 2287−2298.

(9) Lai, S. L.; Carlsson, J. R. A.; Allen, L. H. Melting Point Depression of Al Clusters Generated During the Early Stages of Film Growth: Nanocalorimetry Measurements. *Appl. Phys. Lett.* **1998**, *72*, 1098−1100.

(10) Sun, J.; Simon, S. L. The Melting Behavior of Aluminum Nanoparticles. *Thermochim. Acta* **2007**, *463*, 32−40.

(11) Schmidt, M.; Kusche, R.; von Issendorff, B.; Haberland, H. Irregular Variations in the Melting Point of Size-Selected Atomic Clusters. *Nature* **1998**, *393*, 238−240.

(12) Aguado, A.; Jarrold, M. F. Melting and Freezing of Metal Clusters. *Annu. Rev. Phys. Chem.* **2011**, *62*, 151−72.

(13) Schmidt, M.; Kusche, R.; Kronmüller, W.; von Issendorff, B.; Haberland, H. Experimental Determination of the Melting Point and Heat Capacity for a Free Cluster of 139 Sodium Atoms. *Phys. Rev. Lett.* **1997**, *79*, 99−102.

(14) Breaux, G. A.; Benirschke, R. C.; Sugai, T.; Kinnear, B. S.; Jarrold, M. F. Hot and Solid Gallium Clusters: Too Small to Melt. *Phys. Rev. Lett.* **2003**, *91*, 215508.

(15) Chirot, F.; Feiden, P.; Zamith, S.; Labastie, P.; L'Hermite, J.-M. A Novel Experimental Method for the Measurement of the Caloric Curves of Clusters. *J. Chem. Phys.* **2008**, *129*, 164514.

(16) Breaux, G. A.; Neal, C. M.; Cao, B.; Jarrold, M. F. Melting, Premelting, and Structural Transitions in Size-Selected Aluminum Clusters with around 55 Atoms. *Phys. Rev. Lett.* **2005**, *94*, 173401.

(17) Neal, C. M.; Starace, A. K.; Jarrold, M. F. Melting Transitions in Aluminum Clusters: The Role of Partially-Melted Intermediates. *Phys. Rev. B: Condens. Matter Mater. Phys.* **2007**, *76*, 054113.

(18) Jarrold, M. F.; Cao, B.; Starace, A. K.; Neal, C. M.; Judd, O. H. Metal Clusters that Freeze into High Energy Geometries. *J. Chem. Phys.* **2008**, *129*, 014503.

(19) Hock, C.; Bartels, C.; Straßburg, S.; Schmidt, M.; Haberland, H.; von Issendorff, B.; Aguado, A. Premelting and Postmelting in Clusters. *Phys. Rev. Lett.* **2009**, *102*, 043401.

(20) Cao, B.; Starace, A. K.; Judd, O. H.; Bhattacharyya, I.; Jarrold, M. F. Metal Clusters with Hidden Ground States: Melting and Structural Transitions in $Al_{115}^+$, $Al_{116}^+$, and $Al_{117}^+$. *J. Chem. Phys.* **2009**, *131*, 124305.

(21) Kusche, R.; Hippler, Th.; Schmidt, M.; von Issendorff, B.; Haberland, H. Melting of Free Sodium Clusters. *Eur. Phys. J. D* **1999**, *9*, 1−4.

(22) Schmidt, M.; Donges, J.; Hippler, T.; Haberland, H. Influence of Energy and Entropy on the Melting of Sodium Clusters. *Phys. Rev. Lett.* **2003**, *90*, 103401.

(23) Schmidt, M.; Haberland, H. Phase Transitions in Clusters. *C. R. Phys.* **2002**, *3*, 327−340.

(24) Zamith, S.; Labastie, P.; Chirot, F.; L'Hermite, J.-M. Two-Step Melting of $Na_{41}^+$. *J. Chem. Phys.* **2010**, *133*, 154501.

(25) Breaux, G. A.; Hillman, D. A.; Neal, C. M.; Benirschke, R. C.; Jarrold, M. F. Gallium Cluster "Magic Melters. *J. Am. Chem. Soc.* **2004**, *126*, 8628−8629.

(26) Breaux, G. A.; Cao, B.; Jarrold, M. F. Second-Order Phase Transitions in Amorphous Gallium Clusters. *J. Phys. Chem. B* **2005**, *109*, 16575−16578.

(27) Krishnamurty, S.; Chacko, S.; Kanhere, D. G.; Breaux, G. A.; Neal, C. M.; Jarrold, M. F. Size-Sensitive Melting Characteristics of Gallium Clusters: Comparison of Experiment and Theory for $Ga_{17}^+$ and $Ga_{20}^+$. *Phys. Rev. B: Condens. Matter Mater. Phys.* **2006**, *73*, 045406.

(28) Neal, C. M.; Starace, A. K.; Jarrold, M. F. The Melting of Alloy Clusters: Effects of Aluminum Doping on Gallium Cluster Melting. *J. Phys. Chem. A* **2007**, *111*, 8056−8061.

(29) Pyfer, K. L.; Kafader, J. O.; Yalamanchali, A.; Jarrold, M. F. Melting of Size-Selected Gallium Clusters with 60−183 Atoms. *J. Phys. Chem. A* **2014**, *118*, 4900−4906.

(30) Neal, C. M.; Starace, A. K.; Jarrold, M. F. Ion Calorimetry: Using Mass Spectrometry to Measure Melting Points. *J. Am. Soc. Mass Spectrom.* **2007**, *18*, 74−81.

(31) Neal, C. M.; Starace, A. K.; Jarrold, M. F.; Joshi, K.; Krishnamurty, S.; Kanhere, D. G. Melting of Aluminum Cluster Cations with 31−48 Atoms: Experiment and Theory. *J. Phys. Chem. C* **2007**, *111*, 17788−17794.

(32) Cao, B.; Starace, A. K.; Neal, C. M.; Jarrold, M. F.; Nunez, S.; Lopez, J. M.; Aguado, A. Substituting a Copper Atom Modifies the Melting of Aluminum Clusters. *J. Chem. Phys.* **2008**, *129*, 124709.




DOI: 10.1021/acs.jpcc.7b02768
*J. Phys. Chem. C* 2017, 121, 10242−10248

(33) Cao, B.; Starace, A. K.; Judd, O. H.; Jarrold, M. F. Phase Coexistence in Melting Aluminum Clusters. *J. Chem. Phys.* **2009**, *130*, 204303.
(34) Starace, A. K.; Neal, C. M.; Cao, B.; Jarrold, M. F.; Aguado, A.; Lopez, J. M. Electronic Effects on Melting: Comparison of Aluminum Cluster Anions and Cations. *J. Chem. Phys.* **2009**, *131*, 044307.
(35) Starace, A. K.; Cao, B.; Judd, O. H.; Bhattacharyya, I.; Jarrold, M. F. Melting of Size-Selected Aluminum Nanoclusters with 84−128 Atoms. *J. Chem. Phys.* **2010**, *132*, 034302.
(36) Shvartsburg, A. A.; Jarrold, M. F. Solid Clusters above the Bulk Melting Point. *Phys. Rev. Lett.* **2000**, *85*, 2530−2532.
(37) Breaux, G. A.; Neal, C. M.; Cao, B.; Jarrold, M. F. Tin Clusters That Do Not Melt: Calorimetry Measurements up to 650K. *Phys. Rev. B: Condens. Matter Mater. Phys.* **2005**, *71*, 073410.
(38) Breaux, G. A.; Benirschke, R. C.; Jarrold, M. F. Melting, Freezing, Sublimation, and Phase Coexistence in Sodium Chloride Nanocrystals. *J. Chem. Phys.* **2004**, *121*, 6502−6507.
(39) Zamith, S.; Labastie, P.; L'Hermite, J.-M. Heat Capacities of Mass Selected Deprotonated Water Clusters. *J. Chem. Phys.* **2013**, *138*, 034304.
(40) Donges, J.; Hippler, Th.; Haberland, H. Influence of Energy and Entropy on the Melting of Sodium Clusters. *Phys. Rev. Lett.* **2003**, *90*, 103401.
(41) Haberland, H.; Hippler, Th.; Donges, J.; Kostko, O.; Schmidt, M.; von Issendorff, B. Melting of Sodium Clusters: Where Do the Magic Numbers Come from? *Phys. Rev. Lett.* **2005**, *94*, 035701.
(42) Hock, C.; Straßburg, S.; Haberland, H.; v. Issendorff, B.; Aguado, A.; Schmidt, M. Melting-Point Depression by Insoluble Impurities: A Finite Size Effect. *Phys. Rev. Lett.* **2008**, *101*, 023401.
(43) Schmidt, M.; Kusche, R.; Hippler, Th.; Donges, J.; Kronmüller, W.; von Issendorff, B.; Haberland, H. Negative Heat Capacity for a Cluster of 147 Sodium Atoms. *Phys. Rev. Lett.* **2001**, *86*, 1191−1194.
(44) Steenbergen, K. G.; Gaston, N. A Two-Dimensional Liquid Structure Explains the Elevated Melting Temperatures of Gallium Nanoclusters. *Nano Lett.* **2016**, *16*, 21−26.
(45) Joshi, K.; Krishnamurty, S.; Kanhere, D. G. "Magic Melters" Have Geometrical Origin. *Phys. Rev. Lett.* **2006**, *96*, 135703.
(46) Susan, A.; Kibey, A.; Kaware, V.; Joshi, K. Correlation Between the Variation in Observed Melting Temperatures and Structural Motifs of the Global Minima of Gallium Clusters: An Ab Initio Study. *J. Chem. Phys.* **2013**, *138*, 014303.
(47) Cao, B.; Starace, A. K.; Judd, O. H.; Jarrold, M. F. Melting Dramatically Enhances the Reactivity of Aluminum Nanoclusters. *J. Am. Chem. Soc.* **2009**, *131*, 2446−2447.
(48) Cao, B.; Starace, A. K.; Judd, O. H.; Bhattacharyya, I.; Jarrold, M. F.; Lopez, J. M.; Aguado, A. Activation of Dinitrogen by Solid and Liquid Aluminum Nanoclusters. *J. Am. Chem. Soc.* **2010**, *132*, 12906−12918.
(49) Cao, B.; Starace, A. K.; Judd, O. H.; Bhattacharyya, I.; Jarrold, M. F. Reactions of Liquid and Solid Aluminum Clusters with $N_2$: The Role of Structure and Phase in $Al_{114}^+$, $Al_{115}^+$, and $Al_{117}^+$. *J. Chem. Phys.* **2014**, *141*, 204304.
(50) Leslie, K. L.; Jarrold, M. F. Dehydrogenation of Benzene on Liquid $Al_{100}^+$. *J. Phys. Chem. A* **2013**, *117*, 2075−2081.
(51) Leslie, K. L.; Shinholt, D.; Jarrold, M. F. Reactions of $CO_2$ on Solid and Liquid $Al_{100}^+$. *J. Phys. Chem. A* **2013**, *117*, 1053−1058.
(52) Böyükata, M.; Güvenç, Z. B. MD Study of Energetics, Melting and Isomerization of Aluminum Microclusters. *Braz. J. Phys.* **2006**, *36*, 720−724.
(53) Noya, E. G.; Doye, J. P. K.; Calvo, F. Theoretical Study of the Melting of Aluminum Clusters. *Phys. Rev. B: Condens. Matter Mater. Phys.* **2006**, *73*, 125407.
(54) Zhang, W.; Zhang, F.; Zhu, Z. Molecular Dynamics Study on the Melting Phase Transition of Aluminum Clusters with Around 55 Atoms. *Phys. Rev. B: Condens. Matter Mater. Phys.* **2006**, *74*, 033412.
(55) Bagrets, A.; Werner, R.; Evers, F.; Schneider, G.; Schooss, D.; Wölfle, P. Lowering of Surface Melting Temperature in Atomic Clusters with a Nearly Closed Shell Structure. *Phys. Rev. B: Condens. Matter Mater. Phys.* **2010**, *81*, 075435.
(56) Kang, J.; Kim, Y.-H. Half-Solidity of Tetrahedral-like $Al_{55}$ Clusters. *ACS Nano* **2010**, *4*, 1092−1098.
(57) Aguado, A.; López, J. M. Electronic Shell and Dynamical Coexistence Effects in the Melting of Aluminum Clusters: An Interpretation of the Calorimetric Experiments Through Computer Simulation. *J. Phys. Chem. Lett.* **2013**, *4*, 2397−2403.
(58) Vásquez-Pérez, J. M.; Calaminici, P.; Köster, A. M. Heat Capacities from Born−Oppenheimer Molecular Dynamics Simulations: $Al_{27}^+$ and $Al_{28}^+$. *Comput. Theor. Chem.* **2013**, *1021*, 229−232.
(59) Ojha, U.; Steenbergen, K. G.; Gaston, N. $Al_{20}^+$ Does Melt, Albeit Above the Bulk Melting Temperature of Aluminium. *Phys. Chem. Chem. Phys.* **2015**, *17*, 3741−3748.
(60) Alavi, S.; Thompson, D. L. Molecular Dynamics Simulations of the Melting of Aluminum Nanoparticles. *J. Phys. Chem. A* **2006**, *110*, 1518−1523.
(61) Ojwang, J. G.; van Santen, R.; Kramer, G. J.; van Duin, A. C.; Goddard, W. A. Predictions of Melting, Crystallization, and Local Atomic Arrangements of Aluminum Clusters Using a Reactive Force Field. *J. Chem. Phys.* **2008**, *129*, 244506.
(62) Baidyshev, V. S.; Gafner, Y. Y.; Samsonov, V. M.; Bembel, A. G. Modeling Possible Structural Transitions in Aluminum and Lead Nanoclusters. *Crystallogr. Rep.* **2015**, *60*, 95−100.
(63) Starace, A. K.; Neal, C. M.; Cao, B.; Jarrold, M. F.; Aguado, A.; Lopez, J. M. Correlation Between the Latent Heats and Cohesive Energies of Metal Clusters. *J. Chem. Phys.* **2008**, *129*, 144702.
(64) Neal, C. M.; Breaux, G. A.; Cao, B.; Starace, A. K.; Jarrold, M. F. Improved Signal Stability From a Laser Vaporization Source With a Liquid Metal Target. *Rev. Sci. Instrum.* **2007**, *78*, 075108.
(65) Jarrold, M. F.; Honea, E. C. Dissociation of Large Silicon Clusters: The Approach to Bulk Behavior. *J. Phys. Chem.* **1991**, *95*, 9181−9185.
(66) Jarrold, M. F. Dift Tube Studies of Atomic Clusters. *J. Phys. Chem.* **1995**, *99*, 11−21.
(67) Poland, D. Intermediates in the Melting Transitions of Aluminum Nanoclusters. *J. Chem. Phys.* **2007**, *126*, 054507.
(68) Zamith, S.; Chirot, F.; L'Hermite, J. M. A Two-State Model Analysis of the Melting of Sodium Clusters: Insights in the Enthalpy-Entropy Compensation. *Europhys. Lett.* **2010**, *92*, 13004.
(69) Assael, M. J.; Kakosimos, K.; Banish, R. M.; Brillo, J.; Egry, I.; Brooks, R.; Quested, R. N.; Mills, K. C.; Nagashima, A.; Sato, Y.; et al. Reference Data for the Density and Viscosity of Liquid Aluminum and Liquid Iron. *J. Phys. Chem. Ref. Data* **2006**, *35*, 285−300.
(70) Wilson, A. J. C. The Thermal Expansion of Aluminium: Further Experiments. *Proc. Phys. Soc.* **1942**, *54*, 487−491.
(71) Molina, J. M.; Voytovych, R.; Louis, E.; Eustathopoulos, N. The Surface Tension of Liquid Aluminium in High Vacuum: The Role of Surface Condition. *Int. J. Adhes. Adhes.* **2007**, *27*, 394−340.
(72) Tyson, W. R.; Miller, W. A. Surface Free Energies of Solid Metals: Estimation From Liquid Surface Tension Measurements. *Surf. Sci.* **1977**, *62*, 267−276.


DOI: 10.1021/acs.jpcc.7b02768
*J. Phys. Chem. C* 2017, 121, 10242−10248